Surface & Coatings Technology 213 (2012) 59–64

Contents lists available at SciVerse ScienceDirect

Surface & Coatings Technology

journal homepage: www.elsevier.com/locate/surfcoat

Comparative study on the properties of ZnO nanowires and nanocrystalline thin films

E. Broitman [a,*], C. Bojorge [b], F. Elhordoy [c], V.R. Kent [c], G. Zanini Gadioli [d], R.E. Marotti [c], H.R. Cánepa [b], E.A. Dalchiele [c]

[a] Thin Film Physics Division, IFM, Linköping University, SE 581-83 Linköping, Sweden
[b] CINSO, CITEDEF-CONICET, B1603ALO Villa Martelli, Argentina
[c] Instituto de Física & CINQUIFIMA, Facultad de Ingeniería, UdelaR, CP 11000 Montevideo, Uruguay
[d] Instituto de Física Gleb Wataghin, UNICAMP, 13083-970 Campinas, SP, Brazil

ARTICLE INFO

Article history:
Received 15 March 2012
Accepted in revised form 7 October 2012
Available online 13 October 2012

Keywords:
ZnO
ZnO nanowires
Nanocrystalline ZnO
Sol gel
Water adsorption

ABSTRACT

The microstructural, morphological, optical and water-adsorption properties of nanocrystalline ZnO thin films and ZnO nanowires were studied and compared. The ZnO thin films were obtained by a sol–gel process, while the ZnO nanowires were electrochemically grown onto a ZnO sol–gel spin-coated seed layer. Thin films and nanowire samples were deposited onto crystalline quartz substrates covered by an Au electrode, able to be used in a quartz crystal microbalance. X-ray diffraction measurements reveal in both cases a typical diffraction pattern of ZnO wurtzite structure. Scanning electron microscopic images of nanowire samples show the presence of nanowires with hexagonal sections, with diameters ranging from 30 to 90 nm. Optical characterization reveals a bandgap energy of 3.29 eV for the nanowires and 3.35 eV for the thin films. A quartz crystal microbalance placed in a vacuum chamber was used to quantify the amount and kinetics of water adsorption onto the samples. Nanowire samples, which have higher surface areas than the thin films, adsorb significantly more water.

1. Introduction

Nanostructures made of wurtzite ZnO, such as nanowires (NWs) and nanocrystals, are receiving increasing attention because of potential applications in optoelectronic devices, gas sensing elements, detectors, highly efficient photonic devices, near-UV lasers, photovoltaic solar cells, etc. [1–3]. Ü. Özgür et al. and D.C. Look have comprehensively reviewed the properties and applications of ZnO as both, thin film (TF) and nanostructured materials [4,5]. Both publications have stressed the synthesis and application of nanostructured ZnO, such as NWs, nanorods, and nanobelts, because their morphologies and properties can be modified and controlled through synthesis. Size reduction in nanostructured ZnO materials leads to quantum confinement effects, which in turn impart novel electrical, mechanical, chemical, and optical properties to ZnO [6–8]. Another example is the application in photovoltaic solar cells, where the morphology of NW arrays has been observed to improve both the light collection and charge extraction [9,10].

Schmidt-Mende et al. have described a two-step synthesis of ZnO NWs: in the first step the substrate is coated with a seed layer of ZnO nanoparticles; in the second step, NWs are grown on top of the seed layer, which provides nucleation centers [2]. Different deposition methods can be used for each step resulting in nanostructures that have different properties. Chemical vapor deposition and thermal evaporation have been the most commonly used routes for the synthesis of nanocrystalline films, NWs, nanobelts, nanosprings and nanorings, which have been well summarized by Wang [11]. More recently, electrodeposition, sol–gel and other aqueous solution growth techniques have also attracted great interest because they are relatively economical methods that allow growth of nanostructures at low temperatures and over large areas [2,7,12].

Recently we have developed a novel approach to growth of ZnO NWs by a two-step method that combines different techniques [13]. In the first step a seed layer of ZnO nucleation centers is prepared by a sol–gel method; in the second step, NWs are grown on the seed layer by electrochemical deposition. To our knowledge, this was the first time that these two techniques have been combined for ZnO NW preparation [13]. The present study compares the morphology, microstructure, and optical properties of nanostructured ZnO TFs and ZnO NWs grown by this novel technique. Also, the water adsorption at ZnO TF and NW surfaces is measured to compare their surface reactivity.

2. Experimental

2.1. Sample preparation

ZnO TFs and ZnO NWs were grown onto single-crystal quartz substrates of about 1.5 cm^2 area covered by a circular Au electrode, for use in a quartz crystal microbalance (QCM).

* Corresponding author. Fax: +46 13 137568.
E-mail address: esbro@ifm.liu.se (E. Broitman).

0257-8972/$ – see front matter © 2012 Elsevier B.V. All rights reserved.
http://dx.doi.org/10.1016/j.surfcoat.2012.10.015

Films were prepared by sol–gel process from a precursor solution of zinc acetate dehydrate in ethyl alcohol, with deionized water and acetic acid added for the hydrolysis reaction [6,14]. The sol was stirred at 65 °C for 1 h with reflux to become clear and homogeneous. After aging for 24 h at room temperature, ZnO TFs were deposited by spin coating (3000 rpm, 15 s) the sol onto the substrate and then drying at 150 °C for 10 min; four spin coats were applied to obtain thicker films. Samples received a thermal treatment at 370 °C during 3 h to transform the deposited ZnO layers into a nanocrystalline film. Samples were prepared depositing the ZnO TFs on one or both sides of the quartz crystal.

ZnO NWs were electrochemically grown onto the ZnO seed layer deposited on the Au circular electrode side of the quartz crystal. Before growth, acrylic paint was used to mask the back of the quartz crystal and the periphery of the front side of the crystal, leaving an effective NWs coated area of about 0.5 cm^2. The ZnO seed layer was deposited by the same spin coating technique used for the TFs with final heat treatment at 370 °C for 1 h. ZnO NWs were electrochemically grown onto this seed layer. Electrodeposition was performed in a conventional three-electrode electrochemical cell with the substrate as the cathode, a Zn sheet as the counter electrode, and a saturated calomel electrode (SCE) as the reference electrode. The electrolyte was an aqueous solution of the Zn^{+2} precursor (1 mM zinc acetate) and a supporting electrolyte (0.1 M sodium acetate), saturated with bubbling oxygen. The ultra pure water (18 MΩ cm) was provided by a Millipore equipment. ZnO NW arrays were electrodeposited at 70 °C under potentiostatic conditions at −1.000 V vs. SCE for 70 min. The initial pH was adjusted to 6.76. The final sample was washed with deionized water to remove any residual salt [13].

2.2. Sample characterization

Structural characterization of the ZnO TFs and ZnO NW arrays was performed by X-ray diffraction (XRD) using a Philips PW3710 diffractometer with CuK_α radiation operating with grazing angle geometry (GIXRD) at a constant incidence angle $\alpha_i = 1°$. Scanning electron microscopy (SEM) images were obtained with a LEO 1550 SEM equipment operated at 5 kV.

The optical properties of the samples were studied by diffuse reflectance spectroscopy rather than transmittance spectroscopy due to the optically opaque Au back contact [15]. A 1000 W electric power Xe lamp (ORIEL 6271) light source was used for this measurement. The light was chopped with an SRS SR540 chopper and monochromated with an ORIEL 77250 monochromator. The reflected light (normal detection and quasi-normal incidence [16]) was detected by a UV enhanced unbiased silicon detector of 100 mm^2 area (UDT 11-09-001-1). A first lock-in amplifier (SRS SR530) extracted the signal from the detector, while a second lock-in amplifier (EG&G 5209) was used to measure the variation of the optical source amplitude, correcting its variations in the first lock-in through the ratio output. A PC controlled the entire process (monochromator movement and GPIB communication with the lock-in). Measurements were performed at room temperature.

2.3. Water adsorption measurement on ZnO TFs and NWs

The apparatus designed and constructed for measurement of water vapor adsorption onto ZnO films has been described previously [17,18]. It consists of a vacuum chamber that can be evacuated by either a turbopump or a sorption pump and operates in the pressure range of 10^{-6}–10^4Torr. The turbopump was used to achieve an initial base pressure of 10^{-6}Torr; the sorption pump was used during the experiments to avoid vibrations affecting the microbalance. A capacitance manometer was used to measure the partial pressure of water in the range 10^{-4}–10^4Torr. The QCM housing is capable of holding 3 quartz crystals for simultaneously monitoring of water adsorption on three surfaces. The temperature of the QCM is measured by a K-type thermocouple spot-welded to the quartz crystal housing. The equivalence between %RH and water partial pressure at a given temperature was calculated from the empirical correlation that can be used to estimate the saturated vapor pressure as a function of temperature [19]. A time-resolved QCM-D from Q-Sense with a resolution of 0.01 Hz was used to measure the change in the resonance frequency via a USB interface connected to a computer.

The QCM was used to measure the mass of water adsorbed onto the ZnO TFs and NWs deposited over the gold-coated quartz crystal surface. QCM is a mass sensitive device based on the measurement of the change in resonant frequency of a gold-coated quartz crystal. When water is adsorbed onto these surfaces, the mass change (Δm) can be calculated from the frequency change (Δf) of the crystal resonance by using the Sauerbrey equation:

$$\Delta m = -\frac{A\sqrt{\mu\rho}}{2}\frac{\Delta f}{f_o^2} \quad (1)$$

where f_o is the resonant frequency of the fundamental mode of the crystal, A is the area of the gold disk coated onto the crystal (1.53936 cm^2), ρ is the density of the crystal (2.684 g/cm^3), and μ is the shear modulus of quartz (2.947×10^{11} $g/cm\ s^2$) [20]. Around the resonance frequency of 6 MHz, a net change of 100 Hz corresponds to approximated 6 ng of water adsorbed or desorbed onto the surface of the crystal.

The QCM resonance frequency depends also on the crystal temperature; for our crystals, a change of 0.1 °C corresponds to a frequency change of approximately 0.1 Hz [21]. To avoid artifacts from temperature changes during the experiments, the crystal holder and the chamber were held at a fixed temperature of 50.0 ± 0.1 °C using a temperature-controlled water circulation system [20].

3. Results and discussion

3.1. Morphology

The SEM image of Fig. 1a shows the morphology of a ZnO TF grown onto a single-crystal gold-coated quartz substrate. The surface is relatively smooth, and follows the gold polycrystalline substrate surface. Fig. 1b shows the corresponding morphology of NWs electrodeposited at an electrochemical potential of −1000 mV. The size range of the NWs' diameters is 30 to 90 nm, as indicated in Fig. 1c. The mean size is about 60 nm, with a dispersion of 11 nm, while the most probable value is between 60 and 65 nm. A closer inspection reveals that the NWs have hexagonal section [13], consistent with their wurtzite structure (see Section 3.2). The ZnO NWs grow following the morphology already present in the seed TF layer. This leads to an overall net increase of the sample surface. If we consider that a typical NW has a mean diameter of 62.5 nm and mean length of 500 nm, and that there are 6.88×10^9 nanowires/cm^2 (measured on SEM images), the masked surface of 0.5 cm^2 will have a real surface of about 3.4 cm^2, which corresponds to a surface increase of approximately 7:1.

3.2. Chemical composition and microstructure

Energy-dispersive X-ray spectroscopy analysis (not shown here) has indicated the presence of only two elements, oxygen and Zn, in both TFs and NWs samples.

Fig. 2 shows XRD results for the ZnO samples. The diffraction peaks labeled with an asterisk correspond to the Au layer on the substrate. The X-ray diffraction patterns of TFs and NWs are similar, with diffraction peaks corresponding to the wurtzite (hexagonal) structure of ZnO (space group P63mc) reported for a standard bulk ZnO in the Joint Committee of Powder Diffraction Standards (JCPDS) card file data [22]. No diffraction features characteristics of other phases were detected in the patterns, suggesting that only single-phase ZnO samples

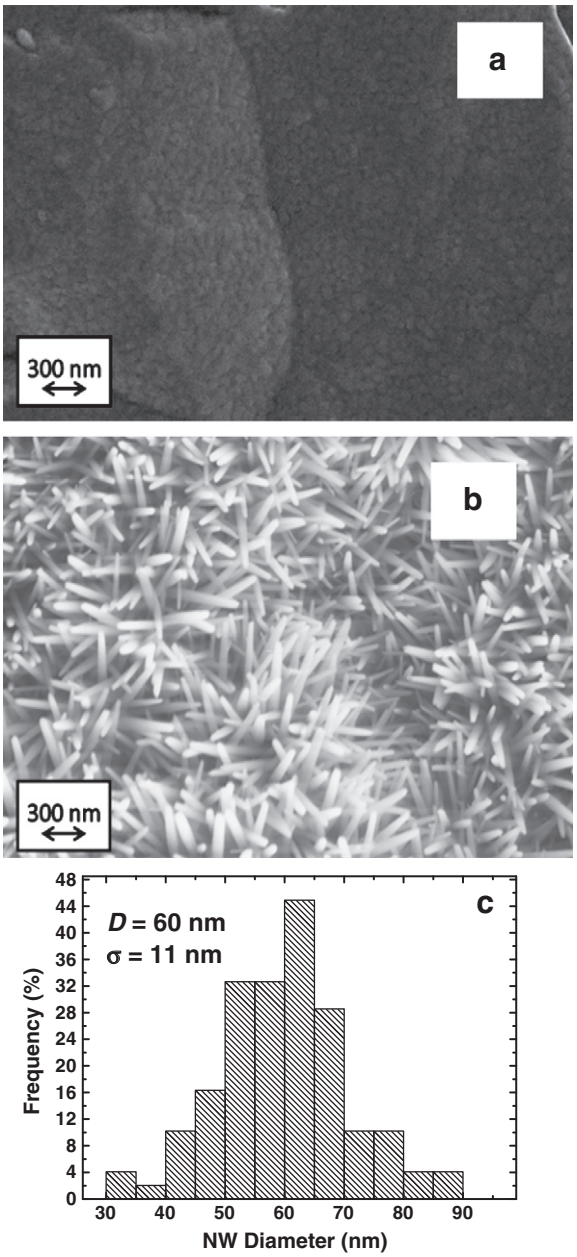

Fig. 1. (a) SEM image of a ZnO thin film deposited onto a single-crystal gold-coated quartz substrate. (b) SEM image of a ZnO NW array electrodeposited at −1000 mV. (c) Corresponding size dispersion, where D is the mean nanowire diameter and σ its standard deviation.

were deposited. The TFs diffraction features are wider than the NWs features, probably due to higher surface stresses and/or smaller crystallite size in the films. Assuming only size broadening (uniform strain within each crystallite), an estimation of crystallite size D can be obtained using Scherrer's equation [23]:

$$D = \frac{k\lambda}{\beta\cos(\theta)} \tag{2}$$

where the constant k is the shape factor close to 1, λ the wavelength of the X-ray, θ the Bragg's angle and β is the full width at half maxima. The XRD peak can be widened by internal stress and defects, so the mean grain size estimated by this method is normally smaller than the actual value [24].

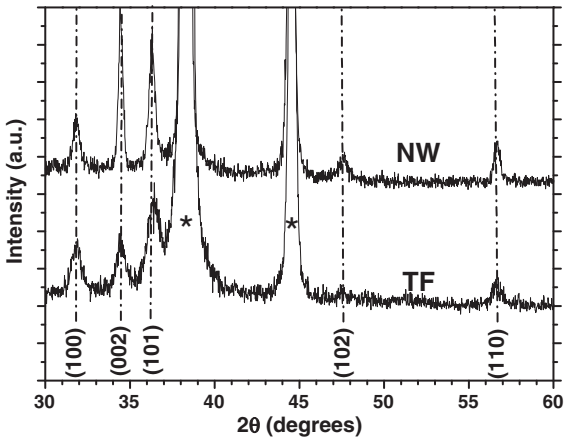

Fig. 2. XRD for TFs (lower curve) and NWs (upper curve). Peaks labeled with "*" are originated from the Au substrate. The vertical dotted lines correspond to the published JCPDS pattern [22].

For the TF samples, the corresponding widths for the (100), (002) and (101) diffraction peaks are 0.637°, 0.552° and 1.065°, respectively. If an instrumental width on the order of 0.3° is taken into account, the grain sizes are in the range of 10 to 33 nm.

For the NWs samples, the corresponding widths for the (100), (002) and (101) diffraction peaks are 0.419°, 0.252° and 0.434°, respectively. The size along the [002] direction is above the range obtainable by this determination, while the widths along the other directions are in the range of 65 to 75 nm, in agreement with the sizes observed by SEM in Fig. 1b and c.

The nanowire exhibits the strongest orientation of the *c*-axis perpendicular to the surface of the substrate, represented by the (002) reflection, suggesting that the nanowires grow along the [002] direction, as we previously reported [13]. The other observed orientations, originated in the beginning of the deposition, are impeded to continue growing whereas it is favored that the growth of NWs aligned perpendicularly to the substrate [25]. Furthermore, the (002) diffraction peak has a relative higher intensity for the NWs than for the TFs (Fig. 2), suggesting a higher texture coefficient along the (002) diffraction peak [26]. The quantification of the texture is, however, difficult because of the vertical shift of the (101) diffraction due to its proximity to a large Au feature.

3.3. Optical properties

Fig. 3 shows the reflectance spectra at different stages of the ZnO NW arrays deposition. All spectra were acquired in the diffuse configuration to improve the spectral features typical of the material. The reflectance spectrum of the quartz substrate with the Au circular electrode is shown in Fig. 3a. The most prominent feature of this spectrum is the absorption edge near 500 nm, which is typical for Au films, giving rise to their characteristic golden color. The reflectance spectrum of the substrate with the seed layer is similar to that of the substrate alone because, with only one spin-coated layer, the film is too thin to be detected.

Fig. 3b shows the spectrum (full line) for the ZnO TFs prepared by the four layer sol–gel spin coating technique. The Au feature is still present, but another feature, attributed to the ZnO, appears between 350 and 400 nm. The first derivative of the spectrum (dR/dλ, short dashed line in Fig. 3b) displays two prominent features. The first feature is due to the Au electrode of the substrate. The second feature at 370 nm (3.35 eV) is very close to bandgap energy of bulk ZnO (most accepted value $E_g = 3.3$ eV [4] and usually reported between 3.2 and 3.4 eV [27]).

Fig. 3c shows the corresponding spectrum for ZnO NW arrays. Although the feature due to Au electrode is still present, a more clear and typical absorption edge, due to ZnO, appears near 380 nm [15]. The derivative of the spectrum dR/dλ displays a clear peak that

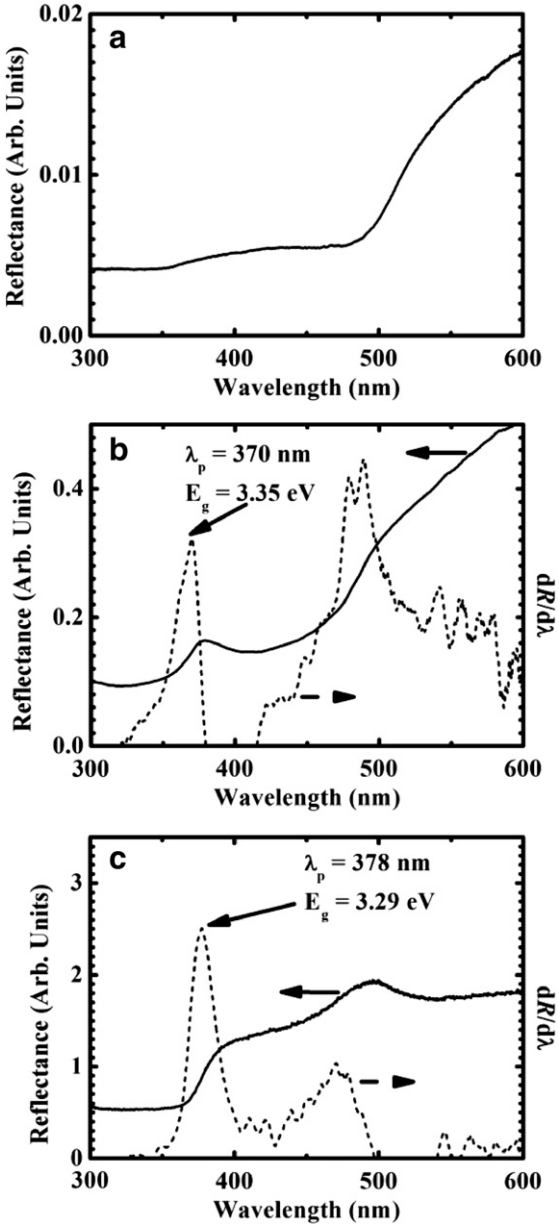

Fig. 3. Optical properties of (a) substrate (Au electrode deposited onto quartz substrate), (b) ZnO TF deposited onto substrate by four-layer spin coating, and (c) ZnO NW arrays electrodeposited at −1000 mV. In (b) and (c), the full lines are the reflectance spectra while short dotted lines are the first derivative against wavelength.

indicates a direct semiconductor band edge [28,29], as expected for ZnO [15]. The bandgap energy value obtained from this peak position is 3.29 eV, also in agreement with usually reported values for ZnO [4,27]. Note that the bandgap for the NW sample is smaller than that of the TF (Fig. 3b), and also that the shape of the ZnO feature of Fig. 3b is slightly different from the clear edge of Fig. 3c. These differences may be due to quantum confinement effects related to the nanocrystalline structure of the TF [30]. Based on both the nanowire diameters obtained from SEM (Fig. 1) and the corresponding nanocrystallite sizes obtained from XRD peak widths (Fig. 2), we confirm that NWs have nanometric sizes ten-times larger than ZnO exciton radius (~2 nm [4]). Therefore, we would expect the NWs' bandgap energies and optical properties to be closer to those of the bulk material. The smaller crystallite sizes estimated for TF (as obtained from XRD peak widths) correspond with the blue shift absorption edge, as observed in Fig. 3b.

3.4. Water adsorption

Fig. 4 shows, in the left vertical axis, the change in resonant frequency Δf for ZnO TFs (one and two-side coated crystals), and ZnO NW coated crystals as a function of the water vapor pressure. The decrease in Δf with the increase of relative humidity can be correlated to the adsorption of water vapor on the TF and the NW surfaces.

The difference in adsorption between one and two-sided ZnO TF samples can be related to the difference in adsorption properties for ZnO TFs and the back surface of the quartz crystal. The data show that ZnO TFs adsorb more water than quartz. The information from both samples has been used to calculate the adsorption properties of ZnO NWs samples that did not have a coated backside.

The interaction of water with ZnO surfaces is still poorly understood in part due to the complex mechanism of water adsorption on metal oxide surfaces, such as ZnO [31]. However, this effect has been already proposed to be used in the design of humidity sensors based on ZnO bulk [32], TFs [33,34], NWs, [35,36] nanorods, [37,38] and nanotubes [39].

It has been shown [40–44] that ZnO films and NWs have surface defects, such as electron vacancies, oxygen vacancies, and interstitial Zn atoms in the surface lattice. These defects can interact with H^+ ions and hydroxyls OH^- dissociated from the H_2O molecules through the following reactions:

$$2H_2O \rightarrow H_3O^+ + OH^- \quad (3)$$

$$H_3O \rightarrow H_2O + H^+. \quad (4)$$

Meyer et al. calculated that the dissociation barrier for water is very small, allowing for an autodissociation even at low temperatures [43]. According to these models [41–44], we can assume that the first step of adsorption in the material will be chemisorption, while the next step will be physisorption of water molecules on top of the chemisorbed layer, as shown in Fig. 5. We have recently confirmed this assumption by, to our knowledge, the only temperature programmed desorption (TPD) experiment of water on nanocrystalline ZnO TF [6].

The right vertical axis of Fig. 4 shows a water surface density scale, calculated by the use of the geometric area of the quartz crystal (1.53936 cm2). In all three samples the increase of water surface density is not a linear function of water vapor pressure. For nanostructured ZnO films deposited by thermal evaporation, a similar non-linear relationship has been explained by the BET model, suggesting a

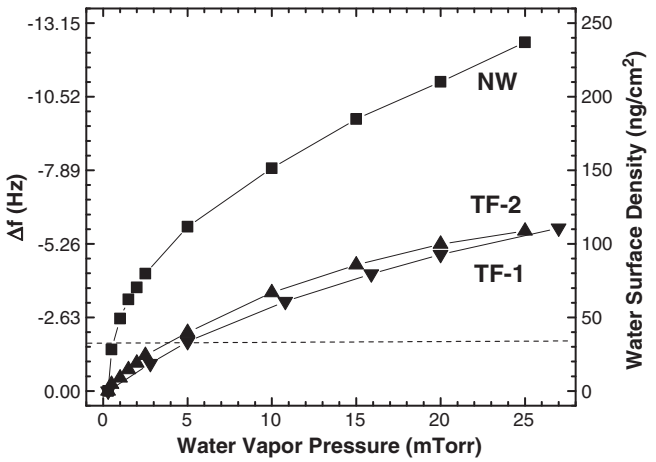

Fig. 4. Water adsorption versus water pressure for (a) one side ZnO TF coated substrate; (b) two-sides ZnO TF coated substrate; (c) one-side ZnO NW coated substrate. The left vertical axis shows the decrease in resonant frequency Δf of the quartz crystal, and the right vertical axis shows a water surface density scale, calculated by the use of the geometrical area of the quartz crystal. The dashed line indicates one monolayer of water coverage on a perfect flat surface (33 ng/cm^2).

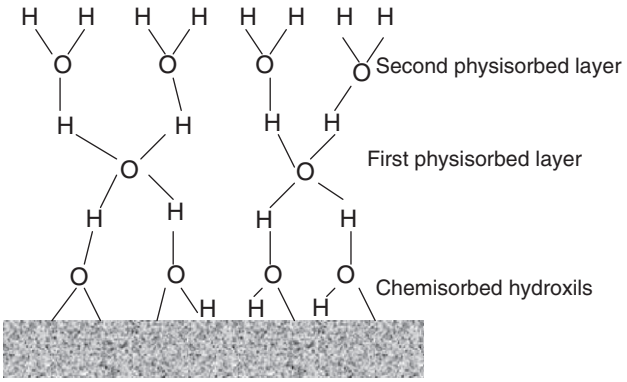

Fig. 5. Schematic illustration of water adsorption on ZnO surfaces. Adapted from [40].

multi-molecular-layer adsorption [45]. Taking into consideration that one monolayer water coverage on a perfectly flat surface is roughly 33 ng/cm^2 [13,16] and that 10 mTorr of water vapor pressure at 50 °C is equivalent to 20.3% RH, we can estimate that the two-side coated ZnO TF sample adsorbed about 2 monolayers (ML) of water at that ambient humidity, while the NW sample has *apparently* adsorbed 5 ML. The difference in water adsorption can be related to the real surface area of the NW sample, which is significantly larger than the macroscopic surface of the quartz crystal.

At water vapor pressures higher than 15 mTorr, the difference in water surface density between ZnO NWs and TFs is roughly 2:1 (Fig. 4). At these pressures there are multi-molecular-layers of water on both surfaces, and adsorption can be described by the interaction of adsorbed H_2O molecules in adjacent layers. Thus, the difference between the TF and the NW samples is due only to differences in real surface areas: we can conclude the NW sample has about twice the surface area of the TF sample. If we consider that the difference between the TFs and NWs samples originates in a ~0.5 cm^2 region containing nanowires, we can estimate from the results at high pressure in Fig. 4 that the small surface has increased roughly seven times its area. This value agrees well with the estimate from SEM characterization that was described in Section 3.1.

At water vapor pressures lower than 15 mTorr, NWs have a higher sensitivity than the TFs. Erol et al., analyzing QCM results by using a modified Langmuir adsorption isotherm model, have shown that a higher adsorption rate can be correlated to a larger number of available adsorption sites [38]. It has also been shown that ZnO NWs, represented as hexagonal prisms, have a high number of defects on their faceted side-walls [44]. The presence of more active sites to interact with humidity molecules on the walls of the NWs increases their surface reactivity and sensitivity compared to the flat TF samples. As a result, more adsorbed humidity molecules at these active sites cause an increase in the adsorption rate at low water vapor pressures.

4. Conclusions

Nanocrystalline ZnO thin films and ZnO nanowires were studied and compared. Both the ZnO thin films obtained by a sol–gel process and the electrochemically grown ZnO nanowires have the same wurtzite structure. Neglecting the influence of strain in XRD peak widths, nanocrystallites with sizes between 10 and 33 nm were obtained for ZnO thin films while elongated shapes with 60 nm mean diameter were obtained for ZnO nanowires grown onto a ZnO sol–gel spin-coated seed layer. SEM morphological studies revealed nanowires with hexagonal sections, consistent with their hexagonal wurtzite structure, and diameters between 30 and 90 nm.

The optical properties of the nanowire array confirm the presence of a direct semiconductor absorption edge, with bandgap energy at 3.29 eV, close to accepted value for ZnO. The optical properties of ZnO thin films (with bandgap energy at 3.35 eV) are influenced by quantum size effects due to the small dimensions of their primary nanocrystalline structure, while the optical properties of ZnO nanowires are not affected due to their relative larger nanometric diameter.

QCM measurements quantified the amount of adsorbed water and adsorption kinetics for ZnO thin films and nanowires. Occupying the same macroscopic area, one-dimensional nanowires adsorbed larger amounts of water because they have a higher surface-to-volume ratio than thin films. ZnO nanowires are more sensitive to low water vapor pressures (i.e., low %RH) than ZnO thin films, likely due to a higher number of defects on their walls.

Acknowledgments

This work was partially supported by the CNPq (Brazil, Prosul Program, Project # 490580/2008-4) and CLAF. The authors gratefully acknowledge helpful discussions with Prof. J.B. Miller from Carnegie Mellon University. E.B. acknowledges the support from the Swedish Government Strategic Research Area Grant in Materials Science, and Prof. A.J. Gellman from Carnegie Mellon University for the use of his QCM adsorption chamber. C.B. thanks M.E.F de Rapp and J. Casanova for their help in XRD experiments and to CITEDEF and CONICET for financial support. F.E., V.R.K., E.A.D. and R.E.M. acknowledge the support received from PEDECIBA–Física, ANII (Agencia Nacional de Investigación e Innovación) and the CSIC (Comisión Sectorial de Investigación Científica) from the Universidad de la República, in Montevideo, Uruguay.

References

[1] Z. Fan, J.G. Lu, J. Nanosci. Nanotechnol. 5 (2005) 1561.
[2] L. Schmidt-Mende, J.L. MacManus-Driscoll, Mater. Today 10 (2007) 40.
[3] D.P. Norton, Y.W. Heo, M.P. Ivill, K. Ip, S.J. Pearton, M.F. Chisholm, T. Steiner, Mater. Today 7 (2004) 34.
[4] Ü. Özgür, Y.I. Alivov, Y.I. Liu, Appl. Phys. Rev. 98 (2001) 041301.
[5] D.C. Look, Mater. Sci. Eng. B 80 (2001) 383.
[6] R.E. Marotti, C.D. Bojorge, E. Broitman, H.R. Canepa, J.A. Badan, E.A. Dalchiele, A.J. Gellman, Thin Solid Films 517 (2008) 1077.
[7] C.N.R. Rao, F.L. Deepak, G. Gundiah, A. Govindaraj, Prog. Solid State Chem. 31 (2003) 5.
[8] B. Sonawane, M. Bhole, D. Patil, Phys. B Condens. Matter 405 (6) (2010) 1603.
[9] B.M. Kayes, H.A. Atwater, N.S. Lewis, J. Appl. Phys. 97 (2005) 114302-1.
[10] J. Tena-Zaera, Jamil Elias, C. Lévy-Clément, Appl. Phys. Lett. 97 (2008) 233119-1.
[11] Z.L. Wang, MRS Bull. 32 (2007) 109.
[12] V. Shelke, M. Bhole, D. Patil, Solid State Sci. 14 (6) (2012) 705.
[13] C.D. Bojorge, V.R. Kent, E. Teliz, H.R. Canepa, R. Henrıquez, H. Gomez, R.E. Marotti, E.A. Dalchiele, Phys. Status Solidi A 208 (2011) 1662.
[14] L. Armelao, M. Fabrizio, S. Gialanella, F. Zordan, Thin Solid Films 394 (2001) 89.
[15] R.E. Marotti, D.N. Guerra, C. Bello, G. Machado, E.A. Dalchiele, Sol. Energy Mater. Sol. Cells 82 (2004) 85.
[16] S.R. Johnson, T. Tiedje, J. Appl. Phys. 87 (1995) 5609.
[17] E. Broitman, G.K. Gueorguiev, A. Furlan, N.T. Son, A.J. Gellman, S. Stafström, L. Hultman, Thin Solid Films 517 (2008) 1106.
[18] E. Broitman, A. Furlan, G.K. Gueorguiev, Z. Czigany, A.M. Tarditi, A.J. Gellman, S. Stafstrom, L. Hultman, Surf. Coat. Technol. 204 (2009) 1035.
[19] A.L. Buck, J. Appl. Meteorol. 20 (1981) 1527.
[20] E. Broitman, V.V. Pushkarev, A.J. Gellman, J. Neidhardt, A. Furlan, L. Hultman, Thin Solid Films 515 (2006) 979.
[21] M.N. Rocklein, S.M. George, Anal. Chem. 75 (2003) 4975.
[22] JCPDS File 5-0664: ZnO, Joint Committee of Powder Diffraction Standards, 1999.
[23] B. Cullity, Elements of X-ray Diffraction, 2nd ed. Addison Wesley, Reading, MA, 1978.
[24] D. Raoufi, T. Raoufi, Appl. Surf. Sci. 255 (11) (2009) 5812.
[25] O. Lupan, V. Guérin, I. Tiginyanu, V. Ursaki, L. Chow, H. Heinrich, T. Pauporté, J. Photochem. Photobiol.A Chem. 211 (2010) 65.
[26] D. Ariosa, F. Elhordoy, E. Dalchiele, R.E. Marotti, C. Stari, J. Appl. Phys. 110 (2011) 124901.
[27] R. Bhargava, in: EMIS Datareviews Series No 17, London, INSPEC, 1997, p. 27.
[28] G. Riveros, H. Gómez, R. Henríquez, R. Schrebler, R.E. Marotti, E.A. Dalchiele, Sol. Energy Mater. Sol. Cells 70 (2001) 255.
[29] G. Riveros, H. Gómez, R. Henríquez, R. Schrebler, R.E. Marotti, E.A. Dalchiele, Bol. Soc. Chil. Quím. 47 (2002) 411.
[30] C.D. Bojorge, H.R. Cánepa, U.E. Gilabert, D. Silva, E.A. Dalchiele, R.E. Marotti, J. Mater. Sci.: Mater. Electron. 18 (2007) 1119.
[31] Y. Li, F.D. Valle, M. Simonnet, I. Yamada, J.-J. Delaunay, Appl. Phys. Lett. 94 (2009) 023110.
[32] N.K. Pandey, K. Tiwari, Sensors & Transducers J. 122 (2010) 9.
[33] S. Dixit, A. Srivastava, R.K. Shukla, J. Appl. Phys. 102 (2007) 113114.

[34] V. Musat, A.M. Rego, R. Monteiro, E. Fortunato, Thin Solid Films 516 (2008) 1512.
[35] S.-P. Chang, S.-J. Chang, C.-Y. Lu, M.-J. Li, C.-L. Hsu, Y.-Z. Chiou, T.-J. Hsuej, I.-C. Chen, Superlattice. Microst. 47 (2010) 772.
[36] X. Qiu, J. Oiler, J. Zhu, Z. Wang, R. Tang, C. Yu, H. Yu, Electrochem. Solid-State Lett. 13 (2010) J65.
[37] F. Fang, J. Futter, A. Markwitz, J. Kennedy, Nanotechnology 20 (2009) 245502.
[38] Y. Wang, J.T.W. Yeow, L.-Y. Chen, in: G.S. Gupta, Y.R. Huang (Eds.), Recent Advances in Sensing Technology, Springer-Verlag, Berlin, 2009, p. 257.
[39] J. Han, F. Fan, C. Xu, S. Lin, M. Wei, X. Duan, Z.L. Wang, Nanotechnology 21 (2010) 405203.
[40] B.C. Yadav, R. Srivastava, C.D. Dwivedi, Philos. Mag. 88 (2008) 1113.
[41] D. Raymand, A.C.T.v. Duin, D. Spångberg, W.A. Goddard III, K. Hermansson, Surf. Sci. 604 (2010) 741.
[42] B. Meyer, D. Marx, Phys. Rev. B 67 (2003) 035403.
[43] B. Meyer, H. Rabaa, D. Marx, Phys. Chem. Chem. Phys. 8 (2006) 1513.
[44] Y. Dai, Y. Zhang, Y.Q. Bai, Z.L. Wang, Chem. Phys. Lett. 375 (2003) 96.
[45] X. Zhou, J. Zhang, T. Jiang, X. Wang, Z. Zhu, Sensors and Actuators A 135 (2007) 209.